THAI JOURNAL OF PHYSICS, SERIES 10, (2014)

CMB Lensing with Stacked Voids

T. Chantavat[1, 2*] and U. Sawangwit[3]

[1]*ThEP's Laboratory of Cosmology and Gravity*
The Institute for Fundamental Study "The Tah Poe Academia Institute",
Naresuan University, Phitsanulok 65000, Thailand
[2]*Thailand Center of Excellence in Physics, Ministry of Education, Bangkok 10400, Thailand*
[3]*National Astronomical Research Institute of Thailand (NARIT), Chiang Mai 50200, Thailand*

We investigate the potential of using voids as a probe of cosmological parameters through the gravitational lensing effect of the CMB and make predictions for the forthcoming EUCLID survey. By stacking the area, where voids could be observed by EUCLID with PLANCK's CMB data, we have found that the EUCLID survey has the potential to provide constraints on cosmological parameters at accuracies competitive with PLANCK alone and could break degeneracies in some cosmological parameters. We have mode our analysis on what we could optimally expect based on our current knowledge of the stacked void profile and analytical estimates of the void number function. In addition, we also provide a conservative analysis on a pessimistic case where constraints may be significantly degraded by an insufficient number of voids; in this case the inclusion of high-density low-z surveys such as BigBOSS, DES and LSST are required to recover competitive constraints. Stacked CMB lensing with voids will provide a competitive and complimentary route to parameter constraints for the next generation cosmological observations at which point the full potential of this technique can be exploited. Examples of parameter constraints with EUCLID are $100\omega_b = 2.26 \pm 0.01$, $\omega_c = 0.114 \pm 0.002$, $\Omega_\Lambda = 0.684 \pm 0.006$ (optimistic) and $100\omega_b = 2.26 \pm 0.06$, $\omega_c = 0.114 \pm 0.009$, $\Omega_\Lambda = 0.684 \pm 0.026$ (pessimistic + low-z) at 68% confidence level.

Keywords: cosmic background radiation, cosmological parameters, gravitational lensing: weak, large-scale structure of universe

1. INTRODUCTION

Observations of the cosmic microwave background (CMB) of the Universe have provided a wealth of information about the initial conditions and the structure of our early Universe (for a recent review see [1]). Recent observations of the CMB [15, 29] have shown that our Universe is highly Gaussian with nearly scale-invariant power spectrum. This has provided our picture of the Universe as the standard model called the inflationary ΛCDM model [8].

The inflationary ΛCDM model, the Universe is homogeneous and isotropic on large scales. However, on small scales, the hierarchical clustering of matter leads to formations of complex cosmic structure such as clusters of galaxies, walls, filaments and voids [7]. Among these objects, voids occupy a vast majority of space and hence provide the largest volume-based test on theories of structure formation. Recently cosmic voids are being continually found amounting to releases of public void catalogues [26, 34, 36].

The CMB signal from the surface of last scattering has traversed the Universe for 13.8 billion years to reach us, passing through intervening clusters and voids along the line-of-sight. The trajectories of CMB photons are bent towards gravitating matter due to distortion of spacetime caused by gravitational lensing [6]. The gravitational lensing sources distort the CMB temperatures giving rise to the transfer of CMB angular power spectrum to smaller scales [32]. The secondary anisotropies due to lensing effects add cosmological information on the growth of structure and local curvature of the Universe. The scenario is reversed when voids are acting as the sources of gravitational lenses. The de-lensing effect of voids has been investigated in recent literature through the distortions of background galaxies by a stacking method, which enhances the signal [14, 20, 25]. The integrated Sach-Wolfe effect by voids has also been investigated [17, 27]. A precision cosmology with voids is also attainable – the Alcock-Paczyński test could be applied to the morphology of stacked void in order to infer the underlying cosmology with good precisions [22, 33].

The goal of this *article* is to investigate the potential of utilizing voids as probes of cosmology by stacking voids and observing the lensing effect of the CMB, and understand the requirements for the detectability of the effect for the next generation surveys based on the currently proposed EUCLID survey. Throughout this *article*, our fiducial cosmological parameters for Fisher analysis are $\{100\omega_b, \omega_c, \Omega_\Lambda, \Delta^2_{\mathcal{R}}, n_s, \tau\} = \{2.26, 0114, 0.684$

*Corresponding author. Tel: +66(0)55968731
Fax: +66(0)55968737 ; *E-mail*: teeraparbc@nu.ac.th

$2.40\times10^{-9}, 0.971, 0.0851\}$ which is consistent with WMAP9 maximum likelihood cosmological parameters [15]. The matter power spectrum and the angular power spectrum were computed using CAMB[1] [24].

2. THEORY

The formalism for CMB lensing correlations, covariance and Fisher information matrices is given in the context of the flat-sky approximation, which is appropriate for small scale CMB lensing [16]. We advise readers to consult [23] for a complete and rigorous review of recent advancements on the theory of CMB lensing and [3] for a general review of gravitational weak lensing.

2.1 CMB Lensing – Flat sky approximation

We consider a lensed CMB temperature anisotropy in the direction $\hat{n}$ on the sky, $\tilde{\Theta}(\hat{n})$ and an unlensed temperature anisotropy $\tilde{\Theta}(\hat{n}+\alpha)$ where α is the deflection angle due to a source with lensing potential $\psi(\hat{n})$, $\alpha \equiv \nabla\psi(\hat{n})$. $\tilde{\Theta}(\hat{n})$ can be expanded as

$$\tilde{\Theta}(\hat{n}) = \Theta(\hat{n}) + \nabla_i\psi\nabla^i\Theta(\hat{n}) + \frac{1}{2}\nabla_i\psi\nabla_j\psi\nabla^i\nabla^j\Theta(\hat{n}) + O(\psi^3). \quad (1)$$

The Fourier transform of Eq. (1) is

$$\tilde{\Theta}(\boldsymbol{\ell}) = \Theta(\boldsymbol{\ell}) - \int \frac{\mathrm{d}^2\ell_1}{(2\pi)^2}\Theta(\boldsymbol{\ell}_1)L(\boldsymbol{\ell},\boldsymbol{\ell}_1), \quad (2)$$

where the lensing kernel $L(\boldsymbol{\ell},\boldsymbol{\ell}_1)$ is given by

$$L(\boldsymbol{\ell},\boldsymbol{\ell}_1) = \psi(\boldsymbol{\ell}-\boldsymbol{\ell}_1)(\boldsymbol{\ell}-\boldsymbol{\ell}_1)\cdot\boldsymbol{\ell}_1 - \frac{1}{2}\int\frac{\mathrm{d}^2\ell_2}{(2\pi)^2}\psi(\boldsymbol{\ell}_2)\psi(\boldsymbol{\ell}-\boldsymbol{\ell}_1-\boldsymbol{\ell}_2)(\boldsymbol{\ell}_1\cdot\boldsymbol{\ell}_2) \times(\boldsymbol{\ell}_1\cdot(\boldsymbol{\ell}-\boldsymbol{\ell}_1-\boldsymbol{\ell}_2)). \quad (3)$$

$\Theta(\hat{n})$ is assumed Gaussian distributed. Therefore, the only independent correlation function is the two-point correlation function,

$$\langle\Theta(\boldsymbol{\ell})^*\Theta(\boldsymbol{\ell}')\rangle = (2\pi)^2\delta_D^2(\boldsymbol{\ell}-\boldsymbol{\ell}')C_\ell^{\Theta\Theta}, \quad (4)$$

where $\delta_D^2(\boldsymbol{\ell}-\boldsymbol{\ell}')$ is the 2D Dirac's delta function and $C_\ell^{\Theta\Theta}$ is the $\Theta\Theta$-multipole moment of the order ℓ. From Eqs. (2) – (4)

$$\tilde{C}_\ell^{\Theta\Theta} = C_\ell^{\Theta\Theta}\left[1 - \int\frac{\mathrm{d}^2\ell_1}{(2\pi)^2}(\boldsymbol{\ell}\cdot\boldsymbol{\ell}_1)^2 C_{\ell_1}^{\psi\psi}\right] + \int\frac{\mathrm{d}^2\ell_1}{(2\pi)^2}(\boldsymbol{\ell}_1\cdot(\boldsymbol{\ell}-\boldsymbol{\ell}_1))^2\left[C_{\ell_1}^{\Theta\Theta}C_{|\boldsymbol{\ell}-\boldsymbol{\ell}_1|}^{\psi\psi} + C_{\ell_1}^{\Theta\psi}C_{|\boldsymbol{\ell}-\boldsymbol{\ell}_1|}^{\Theta\psi}\right]. \quad (5)$$

The first term in Eq. (5) could be interpreted as a transfer of the angular power spectrum on scale $\boldsymbol{\ell}$ into lensing scale $\boldsymbol{\ell}_1$ while the second term is a consequence of the convolution of Θ power spectrum with the lensing power spectra. Our result is consistent with [16] except for an inclusion of the temperature anisotropy and lensing potential cross-correlation $C_\ell^{\Theta\psi}$.

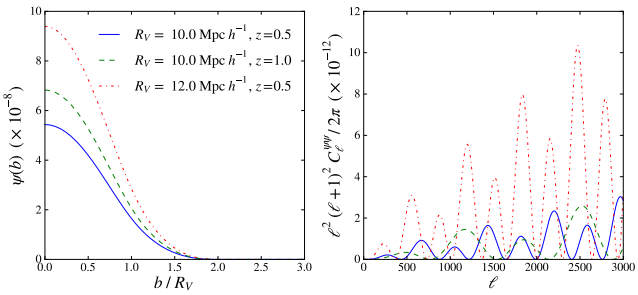

FIGURE 1. The lensing potential of a single void in real space as a function of impact parameter $\boldsymbol{b}\equiv D_K\boldsymbol{\theta}$ where D_K is the commoving angular diameter distance (left) and their corresponding angular power spectra (right) for voids with $R_V = 10.0$ Mpc h^{-1} at $z=0.5$ (solid), $R_V = 10.0$ Mpc h^{-1} at $z=1.0$ (dashed) and $R_V = 12.0$ Mpc h^{-1} at $z=0.5$ (dot-dashed).

2.2 Covariance Matrix and Fisher Analysis

In order to forecast the ability of a given survey to constrain cosmological parameters, we adopt the Fisher matrix formalism [37]. The CMB lensing covariance matrices formalism is adapted from [4] and the bandpower estimator from [32]. The band power estimator for lensed temperature anisotropies is given by

$$\Delta_i^{\tilde{\Theta}\tilde{\Theta}} = \frac{1}{4\pi f_{\mathrm{sky}}\alpha_i}\int_{\boldsymbol{\ell}\in i}\mathrm{d}^2\ell\left(\frac{\ell^2}{2\pi}\right)\tilde{\Theta}^*(\boldsymbol{\ell})\tilde{\Theta}(\boldsymbol{\ell}), \quad (6)$$

where f_{sky} is the fraction of the sky covered by the survey.

$$\alpha_i = \int_{\boldsymbol{\ell}\in i}\mathrm{d}^2\ell, \quad (7)$$

is the integrated ℓ-space area of the ith band power. In this article, we only consider the temperature anisotropy. From the estimator in Eq. (6), the covariance matrix for temperature anisotropy autocorrelation is

$$\mathrm{Cov}(\Delta^{\tilde{\Theta}\tilde{\Theta}},\Delta^{\tilde{\Theta}\tilde{\Theta}})_{ij} = \langle\Delta_i^{\tilde{\Theta}\tilde{\Theta}}\Delta_j^{\tilde{\Theta}\tilde{\Theta}}\rangle - \langle\Delta_i^{\tilde{\Theta}\tilde{\Theta}}\rangle\langle\Delta_j^{\tilde{\Theta}\tilde{\Theta}}\rangle \quad (8)$$

The indices i, j refer to bins in ℓ-space. In term of the covariance matrix, the Fisher matrix is given by

$$F_{\alpha\beta} = \left(\frac{\partial}{\partial p_\alpha}\langle\Delta^{\tilde{\Theta}\tilde{\Theta}}\rangle\right)^T\left(\mathrm{Cov}(\Delta^{\tilde{\Theta}\tilde{\Theta}},\Delta^{\tilde{\Theta}\tilde{\Theta}})\right)^{-1}\left(\frac{\partial}{\partial p_\beta}\langle\Delta^{\tilde{\Theta}\tilde{\Theta}}\rangle\right), \quad (9)$$

where p_α and p_β are cosmological parameters on which the bandpower depends. $\partial\langle\Delta^{\tilde{\Theta}\tilde{\Theta}}\rangle/\partial p_\alpha$ is a column vector of the partial derivative of $\langle\Delta^{\tilde{\Theta}\tilde{\Theta}}\rangle$ with respect to the parameter p_α. To simulate the instrumental noise, we add to the angular power spectra an assumed Gaussian noise for a PLANCK-like CMB[2] survey as explained in details in [11].

[1] http://camb.info

[2] See http://www.rssd.esa.int/index.php?project=planck for PLANCK specifications.

3. VOID AND SURVEY MODELS

We now forecast the sensitivity of stacked CMB lensing of voids on the temperature angular power spectrum of the CMB C_ℓ on the EUCLID survey.

3.1 Void Model

For most voids, the underdense central region is surrounded by an external over dense region called *compensation*. The void profile and the compensation region are not well constrained by current observations. However, the recent simulations of [22] have shown that the radial profile of *stacked* voids is spherically symmetric and is well fitted empirically by

$$\rho_M(x)/\bar{\rho}_M = A_0 + A_3\,(x/R_V)^3\,, \quad \text{for } x < R_V, \qquad (10)$$

where $\bar{\rho}_M$ is the mean cosmic matter density and R_V is the characteristic void radius. The best-fitted parameters are given by $A_0 = 0.13 \pm 0.01$ and $A_3 = 0.70 \pm 0.03$. We ignore the scatter in the best-fitted parameter as it will have negligible impacts on our calculations and employ the top-hat compensated void profile as given in [20]. While large voids do not have such a compensation region [9, 12, 34, 35], their reduced number to not carry significant statistical weight and we will ignore them for this analysis. Some other shapes of compensation regions have been studied in literature (see for example [20])

For a weak gravitational field and a perfect fluid assumption, distortion of spacetime is caused by the Newtonian gravitational potential Ψ_N which obeys the Poisson equation [2],

$$\nabla^2\Psi_N = \frac{4\pi G\bar{\rho}_M}{a}\frac{D(a)}{D(a_0)}\delta_M(a_0), \qquad (11)$$

where ∇ is the commoving gradient operator. $D(a)$ is the linear growth function and a is the scale factor. The gravitational lensing potential $\psi(\hat{n})$ is given by

$$\psi(\hat{n}) = -\frac{2}{c^2}\int \mathrm{d}\chi\, \nabla_\perp\Psi_N(\chi\hat{n}), \qquad (12)$$

where χ is the commoving distance to the lensing source. $\nabla_\perp$ is the transverse derivative. The integral is performed along the line of sight. Similarly, in term of angular separation $\boldsymbol{\theta}$,

$$\psi(\boldsymbol{\theta}) = \int \mathrm{d}^2\hat{n}\left[\sum_i^{N_V}\delta_D^2(\hat{n}-\hat{n}_i)\,\psi_i(\hat{n}_i; R_{V,i}, z_i)\right], \qquad (13)$$

where N_V is the number of voids, $\hat{n}$'s are position of voids in the sky. In the case of stacked voids, the centre of voids are placed along the same line-of-sight. We assume that cross correlation between voids is small [12]. The Fourier transform of the lensing potential into ℓ–space is given by

$$\psi(\boldsymbol{\ell}; R_V, z) = \int \mathrm{d}^2\theta\,\psi(\boldsymbol{\theta}; R_V, z)\exp(-i\boldsymbol{\ell}\cdot\boldsymbol{\theta}). \qquad (14)$$

Figure. 1 shows lensing potential of a stacked void and their corresponding angular power spectra. We have separated the lensing potential into two parts: the stochastic part, ψ_S, and the stacked void part, ψ_V, ie. $\psi = \psi_S + \psi_V$

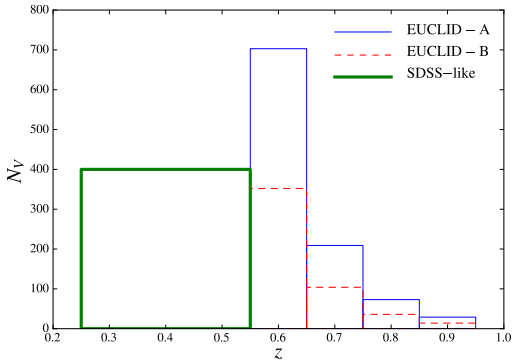

FIGURE 2. The expected number of stacked voids per redshift bin for EUCLID-A (solid), EUCLID-B (dashed) and SDSS-like (thick solid) with approximated characteristic void radius. For the EUCLID survey the bins are $\bar{z} = \{0.6, 0.7, 0.8, 0.9, 1.0\}$ with $\Delta z = 0.1$ and for a futuristic SDSS-like survey, the bin is $\bar{z} = 0.4$ with $\Delta z = 0.15$.

where different parts scale differently which the stacked void number, N_V (See discussion in §5).

3.2 Survey Models

As of the time of writing this article, a theoretical and empirical prediction of number density of voids as a function of mass (or size) and redshift, known as the number function, is not well understood and still a matter of debate [19, 31, 36]. However, for our forecast on stacked CMB lensing signal with voids, we assume the void number function based on simulation as given by [22],

$$\frac{n_V(R_V)}{1\,h^3\,\mathrm{Mpc}^{-3}} = 3.5\times10^{-3}\exp\left(-0.632\frac{R_V}{1\,h^{-1}\mathrm{Mpc}}\right). \qquad (15)$$

With regard to amplifying the signal-to-noise ratio, we follow the stacking procedure as described in [33]. However, the lensing and SZ effects of intervening clusters of galaxies along the line of sight towards voids may attenuate or even contaminate the lensing signature of voids. Hence, we select patches of sky that do not have clusters along the line of sight. For simplicity, we assume that both voids and clusters obey Poisson distribution and the chance of observing such voids can be simply modeled as a survival probability of voids against clusters along the line-of-sight given by [39]

$$P(\bar{z}; f_{\mathrm{patch}}) = \exp\left[-f_{\mathrm{patch}}\int_0^{\bar{z}}\mathrm{d}z\frac{\mathrm{d}N_C}{\mathrm{d}z}(>M_{\mathrm{th}}(z))\right], \qquad (16)$$

where $P(\bar{z}; f_{\mathrm{patch}})$ is the probability of a patch of fractional sky coverage f_{patch} will have a void at redshift $\bar{z}$ without clusters in between. The impact from SZ contamination is expected to be more important than the lensing caused by clusters. Typical angular extension, θ_{500}, of SZ temperature profile is a few $10'$ to $100'$ (see e.g. [28, 38]). All the voids that have at least a cluster within R_V shall be excluded to avoid the angular extension of the SZ effect. $\mathrm{d}N_C/\mathrm{d}z(>M_{\mathrm{th}}(z))$ is the number of clusters with mass greater than threshold mass $M_{\mathrm{th}}(z)$ per redshift bin [10]. [18] mass function is employed in our calculation. In order

to avoid edging effect, we also assume observed square patches with a spherical void with a comparable diameter to the size of the patch residing at the centre.

Our fiducial EUCLID-like survey follows to the most up-to-date simulations of EUCLID's performance at the time of writing [21]. We assume EUCLID spectroscopic survey acquiring a redshift precision of $\sigma_z/(1+z)<0.001$ with sky coverage $f_{\rm sky}=0.4$ and observe galaxies at redshift between $0.5<z<1.5$ for the measurement of lensed CMB sky. The square patches of the survey are assumed to be $0.7°\times0.7°$ which is approximately the field of view of the EUCLID survey. At this stage we are not considering several practical difficulties which may complicate the recognition of voids in the surveys and assume that the surveys can identify voids down to characteristic size of ~ 10 Mpc h^{-1} for EUCLID within the redshift range.

4. RESULTS

We assume a constant mass threshold of $\sim 3.0\times10^{14}M_{\rm sol}h^{-1}$ for EUCLID survey in Eq. (16) as suggested by ACT complete cluster detection limit [13]. However, in our survey model, the number of voids is sensitive to $M_{\rm th}(z)$ and can vary significantly with the mass threshold. The variation of number of stacked voids with $M_{\rm th}(z)$ serves a variety of purposes in our parameterization of the systematic effects upon void detection. Firstly, we are selective on the choice of voids in the stack – only for voids without intervening clusters. However, partially obstructed voids can still be used as long as the major part of voids can be maintained or recovered by removal of the clusters. In this case, $M_{\rm th}(z)$ could be, in principle, increased. Secondly, the accuracy of the void number function in Eq. (15), which has not been tested well with real observations, may alter the number of stacked voids. In order to allow for uncertainties in our prediction, we shall define as optimistic EUCLID survey as EUCLID-A and a pessimistic EUCLID survey, where half of the voids in EUCLID-A are observed, as EUCLID-B. We shall not consider the Poisson uncertainty in the number of detected voids as it is expected to be superseded by other sources of uncertainty mentioned previously.

The low-z voids ($z<0.5$) are still valuable assets since they have already been observed and easily detectable with higher significances in comparison to high-z voids. To complement EUCLID for low-z voids, we shall assume a futuristic SDSS-like survey whose performance is to observed voids in the redshift range $0.3<z<0.5$ with magnitude limit at least $r\approx25.0$ with twice the sky fraction as the contemporary SDSS-III[3] ($f_{\rm sky}\sim0.7$). We assume that the complementary low-z surveys can identify down to voids with characteristic size of ~ 5 Mpc h^{-1}. The lower bound in the redshift range is limited by the fact that voids of size < 4 Mpc h^{-1} are systematically destructed on small scales [22]. The constraint on the magnitude limit is derived form the requirement that the distribution of voids in redshift bin *dim1* and *dim2* samples of [33], where voids of $R_v\sim5$ Mpc h^{-1} are identified, could be observed at $0.3<z<0.5$ and assuming no redshift evolution of voids (See Fig. 1 and 8 in [33]). In other words, the magnitude limit of the survey is adjusted such that the magnitude limit of our target redshift range is the same of that of *dim1*. The sky coverage is set by an extrapolation from our calculation such that EUCLID-B + low-z constraints should be competitive with PLANCK – this requires approximately twice the number of voids with $R_v\sim5$ Mpc h^{-1} in *dim1* + *dim2*. A trade-off between the sky coverage and the magnitude limit of the survey can be easily recognized; however, optimizing the survey is not the main purpose of this article.

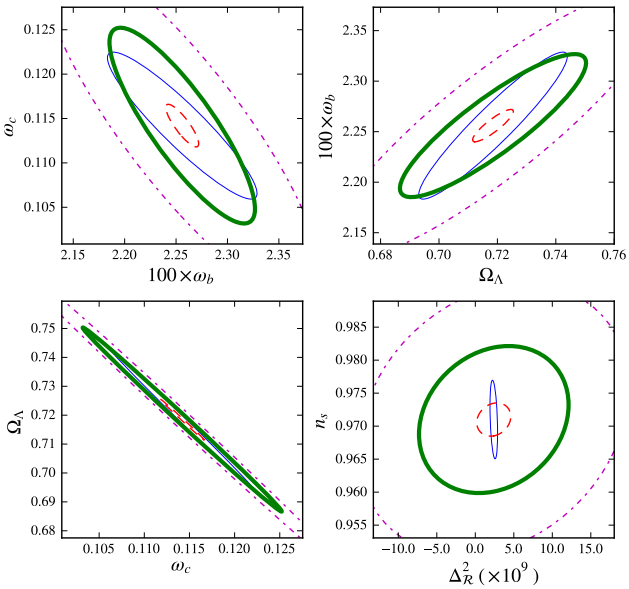

FIGURE 3. 95% CL constraints on some of the cosmological parameter pairs; $100\omega_b$ & ω_c (top-left), Ω_Λ & $100\omega_b$ (top-right), ω_c & Ω_Λ (bottom-left) and $\Delta^2_{\mathcal{R}}$ & n_s (bottom-right) for PLANCK (solid blue), EUCLID-A (dashed red), EUCLID-B (dashed-dotted magenta) and EUCLID-B + (low-z) (thick solid green).

The number of voids per redshift bins used in our calculation is shown in Figure. 2. Our constraints on some of the interesting pairs of cosmological parameters are shown in Figure. 3. In Table 1, 68% confidence level for each of the fiducial cosmological parameters is shown.

5. DISCUSSIONS AND CONCLUSIONS

The main advantage of stacking CMB lensing by voids arises from the fact that the temperature anisotropies are random in nature. For uncorrelated sky regions, the stochastic CMB angular power spectra, when stacked, scale as $\sim1/N_v$. On the contrary, the void lensing power spectra scale as $\sim N_v^2$. The scaling relation of void lensing power

[3] To be compared to Pan-STARRS PS1 $r_{\rm limit}\approx23$, PS2 $r_{\rm limit}\approx24$ and LSST $r_{\rm limit}\approx25$ with $\approx3/4$ sky coverage.

	$100\times\sigma_{\omega_b}$	σ_{ω_c}	σ_{Ω_Λ}	$\sigma_{\Delta^2_{\mathcal{R}}}\times 10^9$	σ_{n_s}	σ_τ
PLANCK	0.0586	0.00667	0.0205	0.396	0.00479	0.0815
EUCLID - A	0.0129	0.00193	0.00561	1.78	0.00203	0.371
EUCILD - B	0.108	0.0158	0.0461	14.1	0.0165	2.949
EUCLID - B + (low-z)	0.0570	0.00888	0.0257	7.82	0.00897	1.63

Table 1
68% CL parameter constraints on the fiducial cosmological parameters for PLANCK, EUCLID-A, EUCLID-B and EUCLID-B + (low-z).

spectra comes from the linearity of the void lensing potential. Therefore, the stacking procedure enhances void power spectra over the intrinsic CMB power spectra by a factor of $\sim N_v^3$. However, the improvement on constraints cannot be infinite due to 1) the cosmic variance; 2) the limitation on the number of voids available; 3) the scatter in the stacked void profile. In this article, only 1) and 2) are considered.

Our survey model is inevitably parameter-dependent, predominantly on $f_{\rm patch}$ and $M_{\rm th}(z)$. The rôle of $M_{\rm th}(z)$ has been discussed in §4. The detection of voids in our case is also sensitive to $f_{\rm patch}$. Increasing $f_{\rm patch}$ reduces the number of voids due to higher chance of encountering clusters and vice verse; however, this allows more ℓ-mode to enter into our Fisher information matrix. In addition, we assume that, regarding to the angular size of the patch at a given redshift, the lensing effect of intervening galaxies are negligible and the effect of removing of the foreground galaxies resulting in the degradation of the effective sky coverage by a factor of a few.

For the optimistic EUCLID-A survey, the overall constraining power is better than PLANCK in almost every cosmological parameters with exception of $\Delta^2_{\mathcal{R}}$ and τ. This is due to the fact that the dependence of the growth function on these parameters is weak. Even though our void profile does not have an explicit dependence on ω_b, the improvement on ω_b is due to the fact that the lensed power spectra with voids are convolution functions of the intrinsic CMB power spectra that depend on ω_b. The general correlation directions differ slightly from PLANCK, but some of the parameters pairs differ significantly and could be used to break the degeneracy with CMB measurements (for example n_s & $\Delta^2_{\mathcal{R}}$). For the pessimistic EUCLID-B survey, the overall constraining power is not competitive with PLANCK. However, with an aide of low-z voids from an SDSS-like survey with high enough sensitivity, the difference in the degeneracy direction are even more pronounced due to the growth rate. This implies that, in order to break the degeneracy with PLANCK effectively, a large number of low-z voids are needed if the pessimistic case is realized.

The other secondary effect besides lensing are notably the Sunyaev-Zel'dovich effect (SZ) [40] and the Rees-Sciama effect (RS) [30]. The SZ effect is expected not to have a sizeable contribution in an underdense region [5]. One would expect that there should be no SZ effect from voids at all as there should be no significant amount of gas. The RS effect, however, will have a significant effect only for large voids.

ACKNOWLEDGMENTS

TC acknowledges the support from the National Astronomical Research Institute of Thailand (NARIT) and Naresuan University grant R2555C018. This work is supported by NARIT research grant and its High Performance Computer facility.

1. Aghanim, N., Majumdar, S., & Silk, J. 2008, Reports on Progress in Physics, 71, 066902
2. Amendola, L., Frieman, J. A., & Waga, I. 1999, MNRAS, 309, 465
3. Bartelmann, M. & Schneider, P. 2001, Phys. Rep., 340, 291
4. Benoit-Lévy, A., Smith, K. M., & Hu, W. 2012, Phys. Rep., 340, 291
5. Birkinshaw, M. 1999, Phys. Rep., 310, 97
6. Blanchard, A. & Schneider, J. 1987, A&A, 184, 1
7. Boylan-Kolchin, M. et al. 2009, MNRAS, 398, 1150
8. Carroll, S. M., Press, W. H., & Turner, E. L. 1992, ARA&A, 30, 499
9. Ceccarelli, L. et al. 2013, MNRAS, 434, 1435
10. Chantavat, T., Gordon, C., Silk, J. 2009, Phys. Rev. D, 79, 083508
11. Chantavat, T., Gordon, C., Silk, J. 2011, Phys. Rev. D, 83, 103501
12. Hamaus, N. et al. 2013, Phys. Rev. Lett., 112, 4
13. Hasselfield, M. et al. 2013, JCAP, 7, 8
14. Higuchi, Y., Oguri, M., & Hamana, T. 2013, MNRAS, 432, 1021
15. Hinshaw, G. et al. 2013 ApJS, 208, 19
16. Hu, W. 2000, Phys. Rev. D, 62, 043007
17. Ilić, S., Langer, M., & Douspis, M. 2013, A&A, 556, A51
18. Jenkins, A. et al. 2001 MNRAS, 321, 372
19. Jennings, E. Li, Y., & Hu, W. 2013, MNRAS, 434, 2164
20. Krause, E. et al. 2013, ApJL, 762, L20
21. Laureijs, R. et al. 2011, arXiv:1110.3193
22. Lavaux, G. & Wandelt, B. D. 2012, ApJ, 754, 109
23. Lewis, A. & Challinor, A. 2006, Phys. Rep., 429, 1
24. Lewis, A., Challinor, A., & Lasenby, A. 2000, ApJ, 538, 473
25. Melchior, P. et al. 2013, arXiv:1309.2045
26. Pan, D. C. et al. 2012, MNRAS, 421, 492
27. Planck Collaboration 2013a, arXiv:1303.5079
28. Planck Collaboration 2013b, arXiv:1303.5089
29. Planck Collaboration 2013c, arXiv:1311.1657
30. Rees, M. J., & Sciama, D. W. 1968, Nature, 217, 511
31. Sheth, R. K., & van de Weygaert, R. 2004, MNRAS, 350, 517
32. Smith, K. M., Hu, W., & Kaplinghat, M. 2006, Phys. Rev. D, 74, 123002
33. Sutter, P. M. et al. 2012a, ApJ, 761, 187
34. Sutter, P. M. et al. 2012b, ApJ, 761, 44
35. Sutter, P. M. et al. 2013a, arXiv:1309.5087
36. Sutter, P. M. et al. 2013b, arXiv:1310.7155
37. Tegmark, M., Taylor, A. N., & Heavens, A. F. 1997, ApJ, 480, 22
38. Whitbourn, J. R., Shanks, T., & Sawangwit, U. 2014, MNRAS, 437, 622
39. White, S. D. M. 1979, MNRAS, 186, 145
40. Zel'dovich, Y. B. 1968, Soviet Physics Uspekhi, 11, 381